

## Decoupling of the magnetic ordering of the rare-earth and the Co sublattice in $\text{Er}_{1-x}\text{Y}_x\text{Co}_2$ compounds driven by substitution or pressure

R. Hauser, E. Bauer, E. Gratz, H. Müller, M. Rotter, H. Michor, and G. Hilscher  
*Institut für Experimentalphysik, T.U. Wien, A-1040 Wien, Austria*

A. S. Markosyan  
*Institute of Physics of AS CR, Cukrovarnickà 10, 162 53 Praha 6, Czech Republic  
 and Faculty of Physics, M.V. Lomonosov Moscow State University, 119899 Moscow, Russia*

K. Kamishima and T. Goto  
*Institute for Solid State Physics, University of Tokyo, Tokyo 106, Japan  
 (Received 14 July 1999)*

The thermodynamic and transport properties of the  $\text{Er}_{1-x}\text{Y}_x\text{Co}_2$  system were studied in the concentration range  $0.0 \leq x \leq 1.0$ . In this system, the first-order magnetic phase transition observed in  $\text{ErCo}_2$  at  $T_C = 32$  K is related to the itinerant electron metamagnetism of the  $d$  subsystem (Co sublattice) driven by the onset of magnetic ordering within the Er sublattice. By employing magnetic, specific heat, thermal expansion, and resistivity measurements we show that in a limited concentration range  $x_{\text{cr}'} < x < x_{\text{cr}}$  and pressure  $P_{\text{cr}'} < P < P_{\text{cr}}$  the itinerant Co sublattice orders magnetically at  $T_C^{\text{Co}}$ , which is lower than  $T_C^{\text{Er}}$  of the Er sublattice. This is referred either to a weakening of the effective molecular field acting on the Co sites owing to the yttrium substitution or to a pressure-driven increase of the critical field necessary to induce a magnetic moment on the Co sites. On further increasing the yttrium concentration or the pressure only the Er sublattice exhibits long-range order. The theoretical calculations within the molecular field approximation are in agreement with the experimental magnetic  $x$ - $T$  phase diagram of the  $\text{Er}_{1-x}\text{Y}_x\text{Co}_2$  system and confirm the effect of a separate ordering of the magnetic sublattices with reasonable parameters used for the intrasublattice Er-Er and inter-sublattice Er-Co exchange interactions. A field-induced collapse of the Co moment, inverse itinerant electron metamagnetism, is well observable by magnetoresistance measurements at appropriate values of concentration and external pressure. The existence of itinerant electron metamagnetism in the Co sublattice is found to be limited in temperature by  $T_0$ , a characteristic temperature which is sensitive to substitution and pressure.

### I. INTRODUCTION

The cubic Laves phase  $R\text{Co}_2$  compounds ( $R$  = rare earth) have been a subject of numerous investigations owing to instability of the Co magnetic state. Compounds with non-magnetic  $R$  (Y, Lu) are exchange-enhanced paramagnets, whereas in those  $R\text{Co}_2$  where  $R$  is a magnetic rare earth a cobalt moment of about  $1\mu_B$  appears in the ordered state.<sup>1</sup>  $\text{YCo}_2$  and  $\text{LuCo}_2$  show a field-induced first-order transition from a paramagnetic to a ferromagnetic state at around  $H_{\text{cr}} \approx 70$  T.<sup>2,3</sup> This phenomenon, a field-induced first-order magnetic transition in an itinerant electron system, also known as itinerant electron metamagnetism (IEM), was first predicted by Wohlfarth and Rhodes<sup>4</sup> for compounds having a highly enhanced Stoner factor and exhibiting a strong energy dependence of the density of states along with a positive curvature in the vicinity of the Fermi level. These conditions for IEM to occur are fulfilled for nearly ferromagnetic  $\text{YCo}_2$  and  $\text{LuCo}_2$  as was shown by band structure calculations.<sup>5</sup>

The first-order magnetic phase transition at  $T_C$  observed in  $\text{ErCo}_2$ ,  $\text{HoCo}_2$  and  $\text{DyCo}_2$  is also ascribed to the metamagnetic behavior of the Co moments, which are magnetized by the internal magnetic field  $H_{fd}^{\text{Co}}$  provided by the rare-earth moments

$$H_{fd}^{\text{Co}} \propto I_{fd}(g_J - 1)J_R, \quad (1)$$

where  $g_J$  is the Landé factor associated with the total angular momentum  $J_R$  of the respective  $R$  element and  $I_{fd}$  is the exchange coupling constant. When plotting the Co moment as a function of  $(g_J - 1)J_R$  for the heavy  $R\text{Co}_2$  series, the metamagnetic behavior of  $M_{\text{Co}}$  can clearly be revealed.<sup>2,6-8</sup>  $H_{fd}^{\text{Co}}$  was found to exceed the critical field of the metamagnetic transition,  $H_{\text{cr}}$ , for all the magnetic  $R$  except for Tm (the contribution of the  $d$ - $d$  exchange interaction to the total molecular field acting on the Co sublattice can be neglected in this series).<sup>9</sup>

Many striking effects were realized in the  $R\text{Co}_2$  compounds when varying the internal parameters. The substitution of  $R$  by Y or Lu results in a reduction of  $H_{fd}^{\text{Co}}$  and a number of studies were concentrated on the properties of  $R_{1-x}\text{Y}_x\text{Co}_2$  and  $R_{1-x}\text{Lu}_x\text{Co}_2$  systems around the concentration where  $H_{fd}^{\text{Co}} \approx H_{\text{cr}}$ .<sup>7,10-18</sup> These studies revealed that for  $R = \text{Er}$ ,  $\text{Ho}$ , and  $\text{Dy}$  the transition at  $T_C$  changes from a first-order towards a second-order type at a critical concentration  $x = x_{\text{cr}'}$ . Above this Y concentration  $H_{fd}^{\text{Co}} < H_{\text{cr}}$  at  $T = T_C$ , which is now the Curie temperature of the  $R$  sublattice only ( $T_C^{\text{R}}$ ). On further cooling,  $H_{fd}^{\text{Co}}$  may still exceed  $H_{\text{cr}}$ . In that case a second magnetic phase transition shall take place where a magnetic moment is induced at the Co sites ( $T_C^{\text{Co}}$ ). Due to the metamagnetic character of the Co ordering, this second magnetic phase transition should be of a first-order

type. With further Y substitution  $T_C^{\text{Co}}$  shall tend towards zero at another critical concentration  $x_{\text{cr}}$ , above which only the  $R$  sublattice will show long-range magnetic order. Therefore, within a limited concentration range  $x_{\text{cr}'} < x < x_{\text{cr}}$  a separate ordering of the two magnetic sublattices can be anticipated.<sup>10</sup> Finally, on further increasing the Y content even long-range magnetic order within the  $R$  sublattice breaks down.

Although the effect of substitution was, e.g., studied in detail in the  $\text{Er}_{1-x}\text{Y}_x\text{Co}_2$  system by Levitin *et al.*,<sup>10</sup> Duc *et al.*,<sup>12</sup> and Baranov *et al.*<sup>13–15</sup> by means of transport and thermodynamic measurements, the existence of such two distinct magnetic phase transitions has not been reported up to now for  $R\text{Co}_2$  compounds. All the data obtained were discussed with respect to a single magnetic phase transition. However, neutron diffraction measurements on this series revealed a coexistence of long-range and short-range order in a limited concentration range.<sup>13</sup> In recent NMR measurements on  $\text{Er}_{1-x}\text{Lu}_x\text{Co}_2$  broad NMR peaks were observed, consisting of two resonance signals, which can suggest a coexistence of both high and low Co moments in a certain range of Lu content.<sup>18</sup>

Concerning the pressure effect on IEM, the experimental data are very limited. Based on an expansion of the free energy, which also takes into account the presence of spin fluctuations, Yamada was able to show that  $H_{\text{cr}}(P)$  has to increase with increasing pressure.<sup>19,20</sup> Furthermore, Yamada showed that metamagnetism finally disappears beyond a critical pressure  $P_{\text{cr}}$ . In the case of  $\text{YCo}_2$  a critical pressure for IEM of about 10–50 kbar was proposed at  $T=0$ , depending on the set of parameters used.<sup>20</sup> He could also show that the possibility for IEM is limited in temperature by a characteristic temperature  $T_0$ ; i.e., there exists a temperature above which the field-induced metamagnetism vanishes.

Assuming that  $H_{fd}^{\text{Co}}$  is not much affected by pressure and that  $H_{fd}^{\text{Co}} \approx H_{\text{cr}}$  at  $T=T_C$ , there shall exist a critical pressure  $P_{\text{cr}'}$  for a change in the character of the magnetic phase transition due to the pressure dependence of  $H_{\text{cr}}$ . Thus, external pressure provides an alternative way for driving the itinerant  $d$  electron subsystem towards magnetic instability. By pressure tuning one can also reach the balance for which

$$H_{\text{cr}}(P,0) < H_{fd}^{\text{Co}} < H_{\text{cr}}(P,T_C). \quad (2)$$

In this particular case, it can be anticipated that starting from a compound which shows a single first-order magnetic transition ( $T_C^R = T_C^{\text{Co}}$ ), within a limited pressure range the Co sublattice will order magnetically at a temperature well separated from that of the magnetic ordering temperature of the  $R$  sublattice.

Of particular interest is also the possibility of inverse IEM and its dependence on substitution or pressure. As the Co moments are coupled antiparallel to those of the heavy  $R$  ions, an external magnetic field  $H_{\text{ext}}$  points opposite to the direction of the Co moments, which are smaller in magnitude than the  $R$  moments. Therefore, above a certain value of the applied magnetic field given by

$$H_{fd}^{\text{Co}} - H_{\text{ext}} \leq H_{\text{cr}}, \quad (3)$$

a sudden collapse of the itinerant Co moment can be expected. This can be treated as an inverse metamagnetic transition at  $H_{\text{ext}} = H_{\text{inv}}$ . This phenomenon was first discussed

and observed by Levitin *et al.*<sup>10</sup> for  $\text{Er}_{1-x}\text{Y}_x\text{Co}_2$  and recently also found for  $\text{Er}_{1-x}\text{Lu}_x\text{Co}_2$  by Bartashevich *et al.*<sup>18</sup> In the case of  $\text{ErCo}_2$  the inverse metamagnetism was detected for  $H_{\text{inv}} = 52$  T.

In the present work we have studied in detail the series  $\text{Er}_{1-x}\text{Y}_x\text{Co}_2$ , in which  $H_{fd}^{\text{Co}}$  can be varied in a controlled way by means of electrical resistivity, specific heat, thermal expansion, and magnetization measurements. Note that in the paramagnetic temperature range clear indications for the presence of strong spin fluctuations in the  $R\text{Co}_2$  compounds are observed,<sup>21</sup> which allows us to study the magnetic state of Co by transport measurements. The goal of the study was to observe experimentally some of the above-discussed phenomena mainly under pressure and to compare our results with the theoretical calculations. Of particular interest was the region around the critical concentration for the onset of the Co magnetic moment (ca.  $x=0.4$ ) where the phase transitions can be induced by comparatively low fields or external pressure.

## II. EXPERIMENTAL DETAILS

Polycrystalline samples of  $\text{Er}_{1-x}\text{Y}_x\text{Co}_2$  were prepared by high-frequency melting under protective argon atmosphere. A ratio of 1:1.93 has been chosen to avoid the formation of the magnetic  $R\text{Co}_3$  phase. Subsequently a heat treatment at 800 °C during 14 days and under argon atmosphere has been applied.

The phase purity of the samples was proved by Debye-Scherrer photographs and x-ray diffraction ( $\text{CrK}\alpha$ ) measurements. The lattice constants of the investigated compounds were determined by using a Siemens D500 diffractometer with Ge as an internal standard. Additionally, the samples were checked by ac- and dc-susceptibility measurements.

The temperature-dependent electrical resistivity was measured on bare-shaped samples in the range  $1.5 \text{ K} < T < 300 \text{ K}$  by means of the conventional four-probe dc technique. Specific heat was measured by a quasiadiabatic step-heat technique in the temperature range 1.5–100 K. Thermal expansion measurements were performed using a capacitance method from 4 K up to room temperature. For magnetization measurements up to 6 T a dc superconducting quantum interference device (SQUID) magnetometer was employed.

The temperature-dependent electrical resistivity was measured under hydrostatic conditions up to 16 kbar by means of a liquid pressure cell, using a 1:4 ethanol-methanol mixture. For higher pressures a Bridgman-type pressure cell was employed with pyrophyllite as gasket and steatite as pressure transmitting medium. In this cell, for pressures less than 20 kbar, the pressure gradient along the measured sample may be as large as 10 kbar. However, on further increasing pressure the conditions inside the cell improve and for pressures more than 20 kbar a gradient less than 3 kbar was deduced from the width of the superconducting transition of the lead manometer. The magnetoresistance data up to 8 kbar and 12 T and down to 0.5 K were obtained employing a Cu-Be pressure cell mounted inside a  $^3\text{He}$  cryostat. Magnetization measurements under hydrostatic pressures up to 13 kbar were performed using an extraction-type magnetometer with a high-pressure clamp made of Cu-Ti alloy in steady magnetic fields up to 9 T.

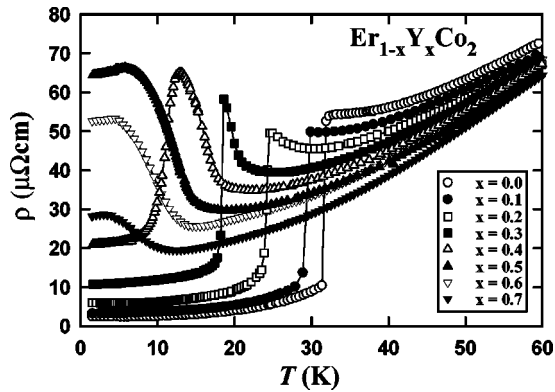


FIG. 1. The temperature-dependent resistivity  $\rho(T)$  of  $\text{Er}_{1-x}\text{Y}_x\text{Co}_2$  compounds for  $x \leq 0.7$ .

### III. EXPERIMENTAL RESULTS

#### A. Ambient pressure data

The temperature-dependent resistivity curves  $\rho(T)$  of the  $\text{Er}_{1-x}\text{Y}_x\text{Co}_2$  system for  $x \leq 0.7$  are shown in Fig. 1. For compounds with  $x \leq 0.3$ , i.e., below the critical Y concentration for the onset of a Co moment, the Curie temperature ( $T_C$ ) is revealed by a steplike discontinuity due to the metamagnetic character of the itinerant electron subsystem. In this concentration region, the peculiar behavior in  $\rho(T)$  just above the Curie temperature can be ascribed to short-range order effects existing in both the sublattices, which enhances the spin-density fluctuations in the Co sublattice due to the  $f$ - $d$  exchange coupling. Hence, a strong increase in  $\rho$  vs  $T$  is observed when approaching  $T_C$  from the paramagnetic temperature range. Below  $T_C$  both magnetic sublattices are ordered and the spin fluctuations in the  $d$  subsystem become suppressed. For the compounds with  $x = 0.5, 0.6$ , and  $0.7$ , in which the Er sublattice only is ordered, the resistivity increases substantially on cooling when approaching  $T_C$  and is almost unaffected by the onset of magnetic order. The intermediate compound  $\text{Er}_{0.6}\text{Y}_{0.4}\text{Co}_2$  shows a distinct behavior. Here magnetic ordering is indicated by a broad maximum, below which the drop in  $\rho(T)$  spreads over several kelvins. This curve combines the features characteristic for both the above described concentration regions.

The temperature variation of the specific heat,  $c_p(T)$ , and the linear thermal expansion  $\Delta l/l(T)$  of some selected compounds of the  $\text{Er}_{1-x}\text{Y}_x\text{Co}_2$  system are shown in Fig. 2. In  $c_p(T)$  a well-defined first-order phase transition is observed only for  $x \leq 0.3$  as can be concluded from the symmetric shape of the respective anomalies. As the volume increase at  $T_C$  is related to the magnitude of the induced Co moment, one can easily read from the thermal expansion data that the onset of the Co moment occurs with the Er/Y substitution in the vicinity of  $x = 0.4$ . The weak anomaly in  $c_p$  recorded for  $\text{Er}_{0.5}\text{Y}_{0.5}\text{Co}_2$  indicates the onset of magnetic order within the diluted Er sublattice only. This is supported by just a small increase in  $\Delta l/l$  on cooling.  $\text{Er}_{0.6}\text{Y}_{0.4}\text{Co}_2$  again shows a particular behavior. Two separate maxima are resolved in  $c_p(T)$  at  $T = 11$  K and  $14.5$  K. In the case of the linear thermal expansion a transition is seen, which is smeared over the temperature interval between  $16$  and  $11$  K, but a considerable volume effect is nevertheless observable.

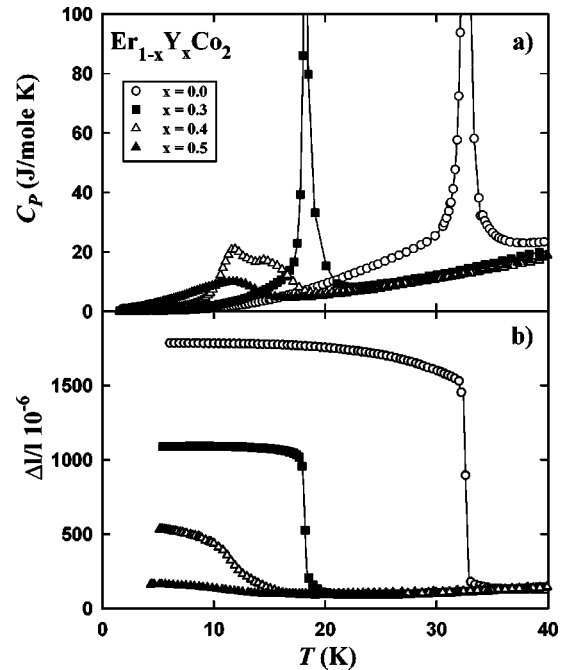


FIG. 2. The temperature-dependent specific heat  $c_p(T)$  (a) and linear thermal expansion  $\Delta l/l(T)$  (b) of  $\text{Er}_{1-x}\text{Y}_x\text{Co}_2$  compounds with  $x = 0, 0.3, 0.4$ , and  $0.5$ .

From the above data one can suggest that two separate magnetic phase transitions occur at least in  $\text{Er}_{0.6}\text{Y}_{0.4}\text{Co}_2$ . In order to reveal the nature of this phenomenon it is worthwhile to compare the magnetic properties of the two compounds  $\text{Er}_{0.6}\text{Y}_{0.4}\text{Co}_2$  and  $\text{Er}_{0.7}\text{Y}_{0.3}\text{Co}_2$ . The temperature dependence of the low-field magnetization  $M(T)$  of these compounds is shown in Fig. 3. The difference observed in  $M(T)$  for the field-cooled (FC) and zero-field-cooled (ZFC) samples is accounted for by a coercivity of these compounds as well as the domain structure. In  $\text{Er}_{0.7}\text{Y}_{0.3}\text{Co}_2$ , the first-order magnetic phase transition is well developed and takes place within a few tenths of a degree. Almost no hysteresis is observed on heating and cooling through  $T_C$  as can be seen from the inset in Fig. 3(a). In contrast, for  $\text{Er}_{0.6}\text{Y}_{0.4}\text{Co}_2$  the increase of magnetization is smeared out over several degrees. The  $M$  vs  $T$  curves for a FC regime at  $1$  mT show two steps, indicating two distinct magnetic phase transitions. A narrow hysteresis for the lower transition can also be observed [see the inset in Fig. 3(b)].

The temperatures of the two magnetic phase transitions found in  $\text{Er}_{0.6}\text{Y}_{0.4}\text{Co}_2$  are compared with that of  $\text{Er}_{0.5}\text{Y}_{0.5}\text{Co}_2$  in Fig. 4, where the temperature derivative of the electrical resistivity ( $\partial\rho/\partial T$ ) and the linear thermal expansion coefficient ( $\alpha$ ) are plotted together. In this presentation, the two transitions observed in  $\text{Er}_{0.6}\text{Y}_{0.4}\text{Co}_2$  can also be resolved by thermal expansion measurements. The sharp maximum at  $11$  K in  $\alpha(T)$  goes along with a first-order phase transition, whereas the steplike behavior around  $14.5$  K points to a second-order phase transition. The first-order type of the low-temperature transition is also in agreement with the hysteresis observed in  $M(T)$  at  $1$  mT centered around  $11$  K [see the inset in Fig. 3(b)]. Thus, for  $x = 0.4$  the Er sublattice orders at a higher temperature ( $T_C^{\text{Er}} = 14.5$  K) than the Co sublattice, which undergoes a separate magnetic transition due to its metamagnetic behavior ( $T_C^{\text{Co}} = 11$  K). Note that

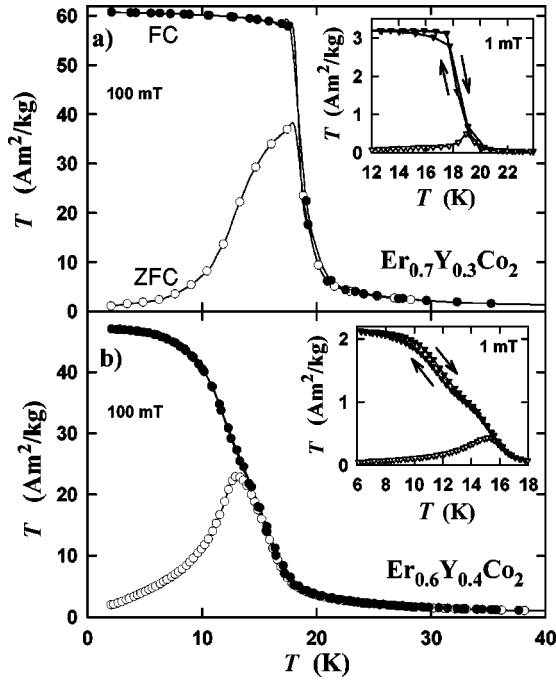


FIG. 3. The thermomagnetic curves  $M(T)$  of  $\text{Er}_{0.7}\text{Y}_{0.3}\text{Co}_2$  (a) and  $\text{Er}_{0.6}\text{Y}_{0.4}\text{Co}_2$  (b) at 10 mT measured on heating. Open and solid symbols denote measurements on zero-field-cooled (ZFC) and field-cooled (FC) samples, respectively. The insets show the magnetization around the magnetic ordering temperatures for an external field of 1 mT on both heating and cooling.

$\partial\rho/\partial T$  also allows us to determine both  $T_C^R$  and  $T_C^{\text{Co}}$  by a minimum and a sharp maximum, respectively. In contrast, for  $\text{Er}_{0.5}\text{Y}_{0.5}\text{Co}_2$  the combined analysis of the thermodynamic and transport data implies one single magnetic phase transition at  $T_C=12.5$  K due to the Er sublattice solely. These results place the critical concentration for vanishing long-range Co ordering within the concentration range  $0.4 < x_{\text{cr}} < 0.5$ .

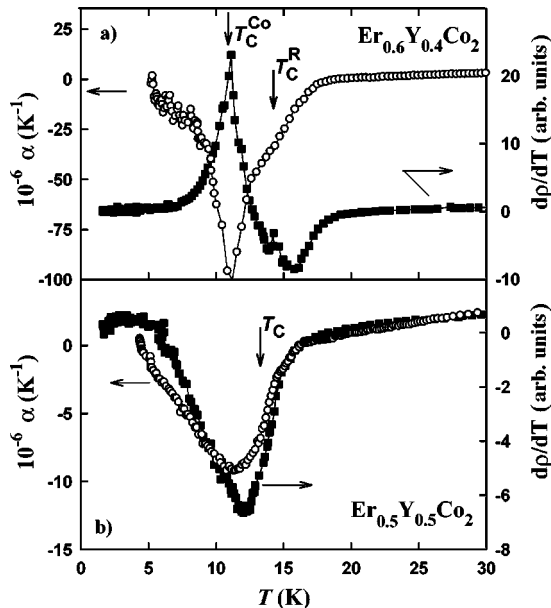


FIG. 4. The thermal expansion coefficient  $\alpha(T)$  and  $\partial\rho/\partial T$  vs  $T$  of  $\text{Er}_{0.6}\text{Y}_{0.4}\text{Co}_2$  (a) and  $\text{Er}_{0.5}\text{Y}_{0.5}\text{Co}_2$  (b) as a function of temperature.

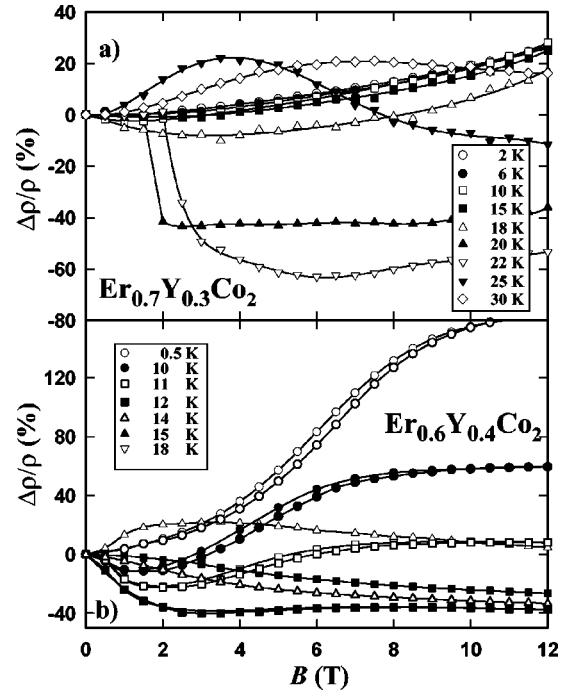


FIG. 5. The magnetoresistance  $\Delta\rho/\rho$  of  $\text{Er}_{0.7}\text{Y}_{0.3}\text{Co}_2$  (a) and  $\text{Er}_{0.6}\text{Y}_{0.4}\text{Co}_2$  (b) at selected temperatures. Note the hysteresis observed for increasing and decreasing magnetic field which, e.g., is indicated by respective arrows for  $T=0.5$  K.

Figure 5 displays the longitudinal magnetoresistance of  $\text{Er}_{0.7}\text{Y}_{0.3}\text{Co}_2$  and  $\text{Er}_{0.6}\text{Y}_{0.4}\text{Co}_2$ . The measurements revealed an irreversible change in the low-temperature resistivity after the application of a moderate field less than 1 T for compounds with  $0.4 \leq x \leq 0.8$  (owing to the change in the domain structure). The initial value is only recovered after heating through  $T_C$  and subsequent zero-field cooling. Nevertheless,  $\Delta\rho/\rho$  was found to be reproducible for further magnetization cycles. For the sake of clarity we only present those data recorded after the initial magnetization cycle. At temperatures where both the magnetic sublattices are ordered, the magnetoresistance increases steadily along with the magnetic field owing to the antiparallel coupling of the localized Er and the induced itinerant Co moments, which causes a progressive demagnetization of the latter sublattice. If the external field is high enough to satisfy Eq. (3), the itinerant Co sublattice must undergo an inverse metamagnetic transition at  $H_{\text{ext}}=H_{\text{inv}}$ . As a consequence,  $\Delta\rho/\rho$  shall increase due to the growing spin-fluctuation scattering. Since for  $x=0.3$  the critical field for inverse IEM is of about 20 T, as shown by magnetostriction measurements,<sup>10</sup> such a behavior is not covered by the field range available. In  $\text{Er}_{0.6}\text{Y}_{0.4}\text{Co}_2$ , in contrast, a drastic increase of magnetoresistance takes place at low temperatures near to 6.5 T [Fig. 5(b)]. A narrow hysteresis is observed around this field-induced anomaly, confirming the first-order type of the transition.  $H_{\text{inv}}$  is broadened over several teslas and is weakly dependent on temperature; its value reduces to  $H_{\text{inv}}=4$  T with increasing temperature up to  $T_C^{\text{Co}}$ .

According to Yamada's theory,<sup>19,20</sup> IEM is limited in temperature by a characteristic temperature  $T_0$ . For  $x=0.3$  and 0.4 the value of  $T_0$  can be read off from the above data. For  $\text{Er}_{0.3}\text{Y}_{0.7}\text{Co}_2$ ,  $\Delta\rho/\rho$  yields a sharp drop above  $T_C$  [Fig. 5(a)],

TABLE I. Experimental values of thermodynamic and transport data of  $\text{Er}_{1-x}\text{Y}_x\text{Co}_2$  compounds. The magnetic ordering temperatures of the  $\text{Er}_{1-x}\text{Y}_x\text{Co}_2$  compounds as deduced from thermodynamic and resistivity measurements.

	$T_C$ (K)	$T_C^R$ (K)	$T_C^{\text{Co}}$ (K)	$T_0$ (K)	$\mu_{\text{Co}}$ ( $\mu_B$ )	$\gamma$ (mJ/mol K)	$\rho_0$ ( $\mu\Omega$ cm)	$H_{\text{inv}}$ (T)
$x=0.0$	32			47	0.97	40	2	52
$x=0.1$	28.9				0.92	—	3	
$x=0.2$	23.7			27	0.80	38	6	
$x=0.3$	18.5			23	0.65	57	11	20
$x=0.4$		14.5	11	13	0.48	87	21	6.5
$x=0.5$		12.5			0.22	204	64	
$x=0.6$		10.0				155	52	
$x=0.7$		7.5				125	28	

in agreement with the isothermal magnetization data of  $\text{ErCo}_2$  and magnetoresistance data on  $\text{Er}_{1-x}\text{Y}_x\text{Co}_2$  by Aleksandryan *et al.*,<sup>11</sup> confirming the metamagnetic behavior in the paramagnetic range. This steplike anomaly is smeared out for  $T > 23$  K, which can be considered as  $T_0$  for  $x = 0.3$ . In  $\text{Er}_{0.6}\text{Y}_{0.4}\text{Co}_2$  the magnetoresistance decreases monotonically in the paramagnetic range without any further sign for inverse IEM. As the isothermal magnetization shows a metamagnetic behavior up to 12 K, it is supposed that for this compound  $T_0$  lies between the two ordering temperatures:  $T_C^{\text{Co}} < T_0 < T_C^R$ . Table I gives some of the characteristic parameters of the  $\text{Er}_{1-x}\text{Y}_x\text{Co}_2$  compounds. The magnetic ordering temperatures deduced from  $\partial\rho/\partial T$  vs  $T$  and from the thermodynamic measurements are in good agreement with each other and with those reported by Levitin *et al.*,<sup>10</sup> Duc *et al.*,<sup>12</sup> and Baranov *et al.*<sup>13–15</sup>  $T_0$  is defined as the temperature up to which a metamagnetic behavior is observed by the magnetoresistance measurements.  $H_{\text{inv}}$  denotes the critical field for inverse IEM,  $\rho_0$  is obtained from the low-temperature resistivity at  $T = 1.5$  K,  $\gamma$  equals the linear term in  $c_p(T)$  and  $\mu_{\text{Co}} = M_{\text{Co}}/2$  is derived from  $\Delta V/V = (\omega_s =) kC\mu_{\text{Co}}^2$  where  $kC$  is the magneto-volume coupling coefficient. The values for  $\omega_s$  were obtained using  $\alpha(T)$  of  $\text{YCo}_2$  as a nonmagnetic reference material and for  $kC \dots 8.14 \times 10^{-3} \mu_B^2/\text{Co}^{-1}$ .<sup>8</sup> The induced itinerant moments thus estimated for  $x \leq 0.4$  are in good agreement with those found in Refs. 10 and 12 and those directly measured by neutron diffraction measurements.<sup>13</sup> Note that  $\rho_0$  and  $\gamma$  start to increase for  $x = 0.3$  and reach maximum at about  $x = 0.5$ . Part of these values have been taken from the literature.<sup>10,12,16,14,15,13</sup>

## B. Pressure data

### 1. Electrical resistivity

The pressure-dependent resistivity of  $\text{ErCo}_2$  at low temperatures (recorded on heating) is given in Fig. 6. Figure 6(a) displays data taken under hydrostatic conditions up to 16 kbar. The pressure-dependent variation of the magnetic-ordering temperature in this range yields  $\partial T_C/\partial P = -0.8$  K/kbar. No clear change in the type of the transition is observed up to 16 kbar. This variation of  $T_C$  vs  $P$  is given in the inset of Fig. 6(a) by solid symbols.

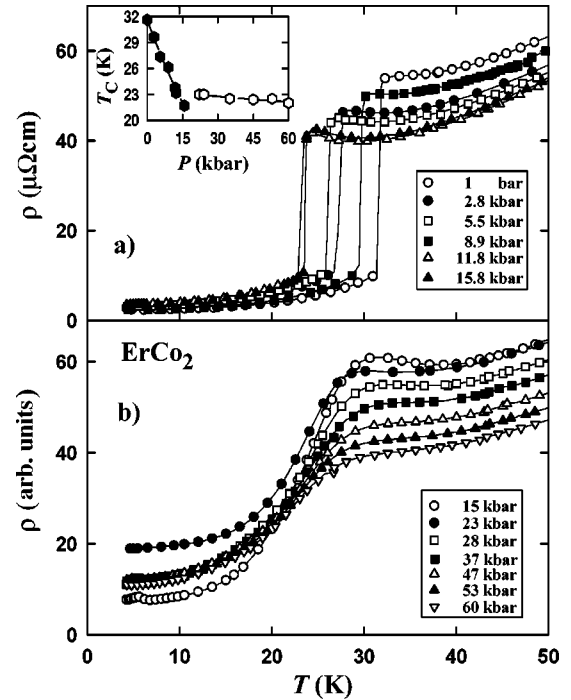


FIG. 6. The temperature-dependent resistivity of  $\rho(T)$   $\text{ErCo}_2$  for pressures up to 60 kbar measured under hydrostatic (a) and quasihydrostatic (b) conditions. The inset shows the pressure dependence of the respective magnetic ordering temperatures (see text).

Figure 6(b) shows the results obtained by means of a Bridgman high-pressure cell up to 60 kbar. Owing to the pressure gradient inherent to this type of cell, the first-order phase transition of  $\text{ErCo}_2$  appears to be ‘‘smeared out’’ over several degrees. Therefore, one neither can give the exact value for one single (smeared first-order or second-order) phase transition nor can even detect a possible splitting into two distinct magnetic phase transitions. Nevertheless, considering the pressure variation of a characteristic point at the drop in  $\rho(T)$  as a measure for  $T_C$  vs  $P$ , a weak pressure dependence is obtained for pressures above 20 kbar [open symbols in the inset of Fig. 6(a)].

The pressure-dependent resistivity of two compounds with an ordered Co sublattice,  $\text{Er}_{0.8}\text{Y}_{0.2}\text{Co}_2$  (a) and  $\text{Er}_{0.7}\text{Y}_{0.3}\text{Co}_2$  (b), is given in Fig. 7. As for  $\text{ErCo}_2$ , in  $\text{Er}_{0.8}\text{Y}_{0.2}\text{Co}_2$  the width of the steplike transition does not change significantly at low pressures. This transition becomes reduced in height and the value of the low-temperature resistivity increases weakly for  $P > 5$  kbar. As was shown above, the splitting of the transition temperatures can be revealed considering the temperature derivative of the resistivity. An analysis of  $\partial\rho/\partial T$  indicates (see the insets) that in  $\text{Er}_{0.8}\text{Y}_{0.2}\text{Co}_2$  a splitting into two magnetic phase transitions occurs above about 10 kbar. For  $\text{Er}_{0.7}\text{Y}_{0.3}\text{Co}_2$ , the joint magnetic ordering of the two sublattices occurring at  $T_C = 18.5$  K was found to become split into two distinct transitions at very low external pressure (less than 1 kbar).

Figure 8 shows the pressure-dependent resistivity of  $\text{Er}_{0.6}\text{Y}_{0.4}\text{Co}_2$  (a) and  $\text{Er}_{0.5}\text{Y}_{0.5}\text{Co}_2$  (b). In  $\text{Er}_{0.6}\text{Y}_{0.4}\text{Co}_2$ , the intermediate compound  $T_C^{\text{Co}}$  vs  $P$  can be traced unambiguously only for pressures up to 1.5 kbar, yielding  $\partial T_C^{\text{Co}}/\partial P = -2.5$  K/kbar. For  $P \geq 3$  kbar the drop of resistivity ex-

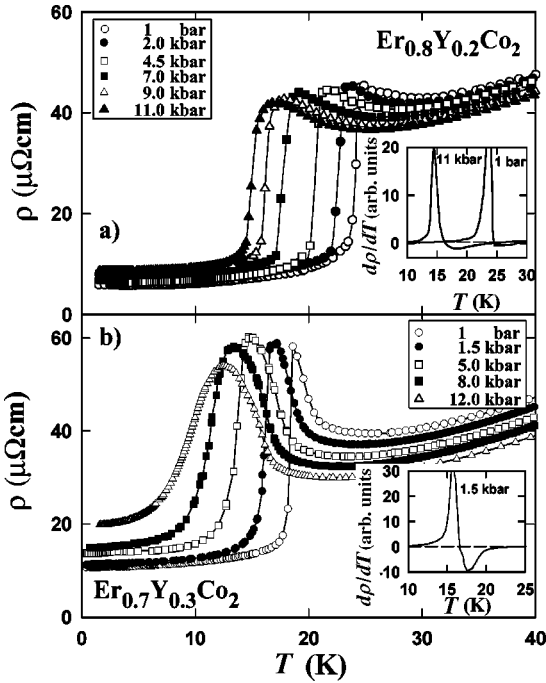


FIG. 7. The temperature-dependent resistivity  $\rho(T)$  of  $\text{Er}_{0.8}\text{Y}_{0.2}\text{Co}_2$  (a) and  $\text{Er}_{0.7}\text{Y}_{0.3}\text{Co}_2$  (b) for pressures up to 15 kbar. The insets show  $\partial\rho/\partial T$  vs  $T$  for selected values of pressure, indicating the splitting of the combined ordering of the two magnetic sublattices above a certain value of pressure.

tends over a wide temperature range and its width in temperature does not change on further increasing pressure. However, the hump in resistivity decreases progressively, a behavior which was also observed at considerably higher pressures for  $\text{ErCo}_2$ . On the other hand  $T_C^R$  vs  $P$  can be traced

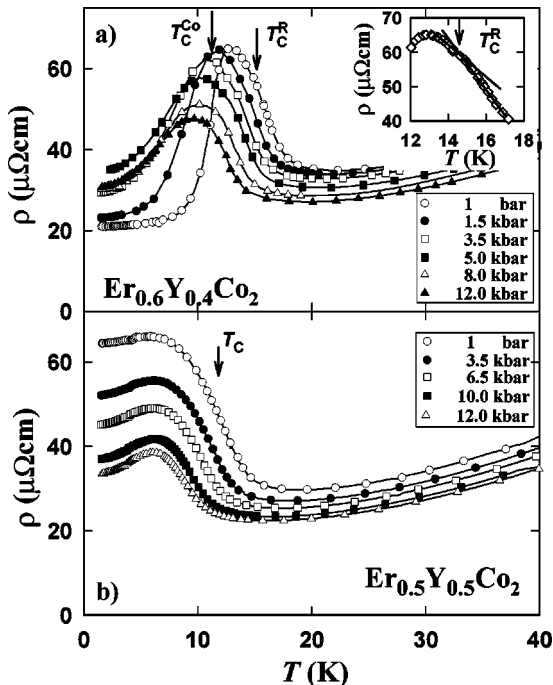


FIG. 8. The temperature-dependent resistivity  $\rho(T)$  of  $\text{Er}_{0.6}\text{Y}_{0.4}\text{Co}_2$  (a) and  $\text{Er}_{0.5}\text{Y}_{0.5}\text{Co}_2$  (b) for pressures up to 15 kbar. The inset shows  $\rho(T)$  around  $T_C^{\text{R}}$  which is indicated by a kink.

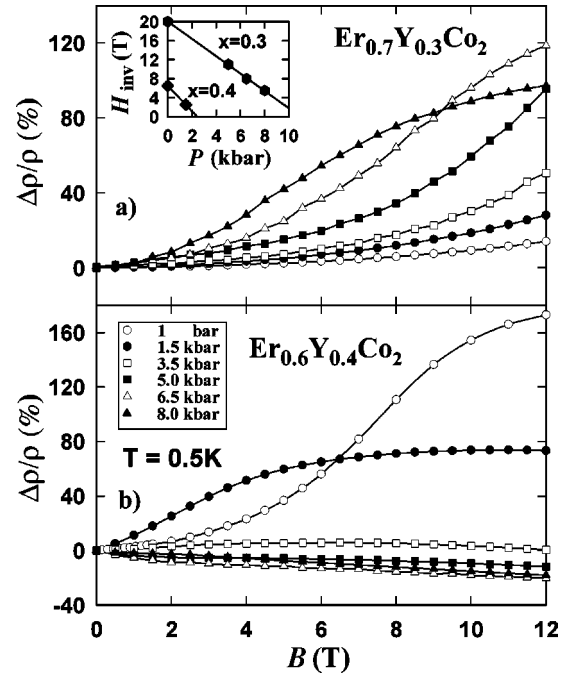


FIG. 9. The magneto-resistance  $\Delta\rho/\rho_0$  of  $\text{Er}_{0.7}\text{Y}_{0.3}\text{Co}_2$  (a) and  $\text{Er}_{0.6}\text{Y}_{0.4}\text{Co}_2$  (b) at  $T = 0.5$  K for pressures up to 8 kbar. The insets show the pressure dependences of the inverse field for IEM,  $H_{\text{inv}}$ .

well from a kink in  $\rho(T)$ , thus giving  $\partial T_C^R/\partial P = -0.35$  K/kbar. Note that  $T_C^R$  can also be revealed by differentiation (see Fig. 4 and the insets of Fig. 7). In  $\text{Er}_{0.5}\text{Y}_{0.5}\text{Co}_2$  where only the  $R$  sublattice orders magnetically,  $T_C = T_C^R = 12.5$  K is again indicated by a small kink in  $\rho$  vs  $T$  in agreement with thermodynamic measurements. Tracing the anomaly in  $\partial\rho/\partial T$  vs  $T$  as a function of pressure yields  $\partial T_C/\partial P = -0.27$  K/kbar for this compound.

## 2. Magneto-resistance

The pressure dependence of IEM can be studied well by magneto-resistance measurements. In Fig. 9 the results for  $\text{Er}_{0.7}\text{Y}_{0.3}\text{Co}_2$  and  $\text{Er}_{0.6}\text{Y}_{0.4}\text{Co}_2$  are given at  $T = 0.5$  K. In the former compound,  $H_{\text{inv}} \approx 20$  T at ambient pressure. However, its value strongly decreases under pressure due to the increase of  $H_{\text{cr}}$ , and above 5 kbar IEM can be observed in fields below 12 T. In  $\text{Er}_{0.6}\text{Y}_{0.4}\text{Co}_2$  ( $H_{\text{inv}} = 6.5$  T at ambient pressure),  $H_{\text{inv}}$  decreases with increasing pressure and reduces to zero above 1.5 kbar. For  $P \geq 3.5$  kbar the Co sublattice does not reveal any long-range magnetic order, and  $\Delta\rho/\rho$  shows a weak negative deviation only. The pressure dependence of  $H_{\text{inv}}$  for both the compounds is shown in the inset of Fig. 9, yielding  $\partial H_{\text{inv}}/\partial P = -1.8$  and  $-3$  T/kbar for  $x = 0.3$  and  $0.4$ , respectively.

In Figs. 10 and 11, the magneto-resistance of  $\text{Er}_{0.7}\text{Y}_{0.3}\text{Co}_2$  is shown under 1.5, 3.5, 5, and 8 kbar pressures at various temperatures. At 5 and 8 kbar the behavior of  $\text{Er}_{0.7}\text{Y}_{0.3}\text{Co}_2$  is very similar to that revealed by the intermediate compound  $\text{Er}_{0.6}\text{Y}_{0.4}\text{Co}_2$  under ambient pressure. The value of  $H_{\text{inv}}$  for inverse IEM decreases with increasing temperature. At 5 kbar a smeared transition centered near 2 T can also be detected at 16 K, i.e., within the temperature interval  $T_C^{\text{Co}} = 13.5$  K  $< T < T_C^{\text{R}} = 16.7$  K, which is now associated with

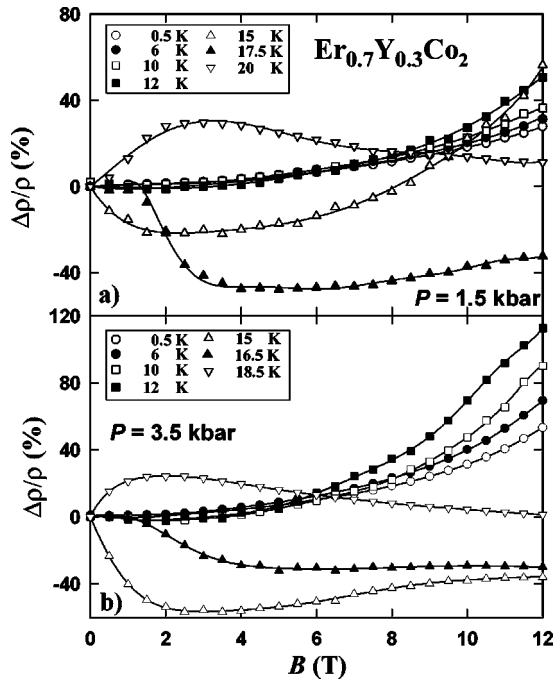


FIG. 10. The magnetoresistance  $\Delta\rho/\rho$  of  $\text{Er}_{0.7}\text{Y}_{0.3}\text{Co}_2$  at 1.5 (a) and 3.5 kbar (b) at various values of temperature.

the onset of the Co magnetic moment due to the positive sign of the  $\partial T_C^{\text{Co}}/\partial H$  derivative. This indicates that the limiting temperature up to which IEM occurs is easily reduced with pressure. One can deduce from these data  $12\text{ K} < T_0 < 16\text{ K}$  for  $\text{Er}_{0.7}\text{Y}_{0.3}\text{Co}_2$  at 5 kbar. At 8 kbar,  $T_0 \approx 11\text{ K}$  was found. Above that temperature no sign of a metamagnetic behavior is observed.

The magnetoresistance of  $\text{Er}_{0.6}\text{Y}_{0.4}\text{Co}_2$  for  $P=1.5$  and 3.5 kbar is shown in Fig. 12. At 1.5 kbar weak indications for

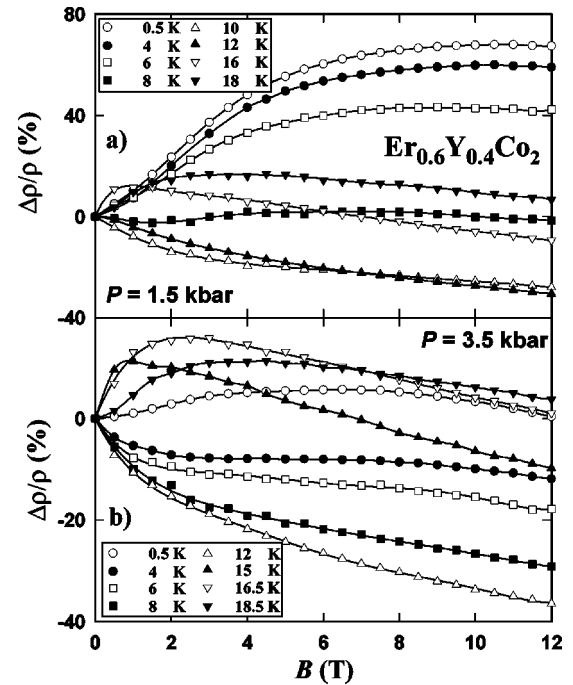


FIG. 12. The magnetoresistance  $\Delta\rho/\rho_0$  of  $\text{Er}_{0.6}\text{Y}_{0.4}\text{Co}_2$  at 1.5 (a) and 3.5 kbar (b) at various values of temperature.

IEM are observed around 2–3 T below  $T < 8\text{ K}$ , which are related to the onset of the Co moment. This differs for 3.5 kbar where the Er sublattice only shows long-range order ( $H_{\text{fd}}^{\text{Co}} < H_{\text{cr}}$  in the ground state). Here and for higher values of pressure no further indication of IEM is observed down to  $T=0.5\text{ K}$ . At elevated temperatures  $\Delta\rho/\rho$  is continuously negative for  $T < T_C^R$  and yields a positive increase at low fields for  $T > T_C^R$ . For  $x=0.4$  we obtain  $\partial T_0/\partial P = -2\text{ K/kbar}$ .

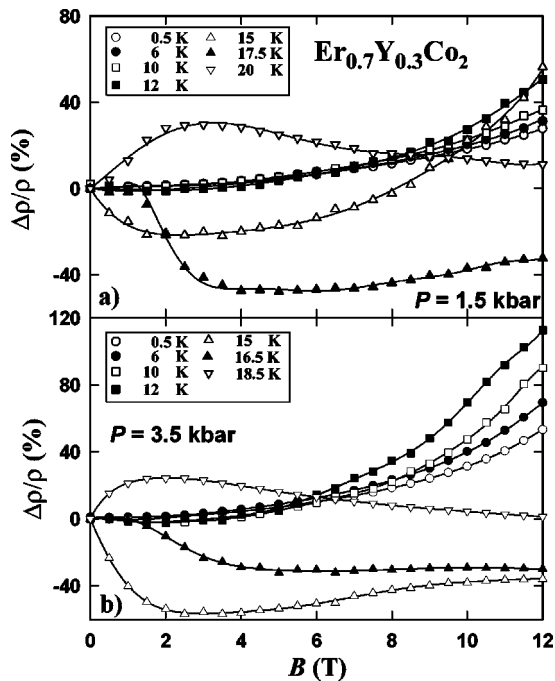


FIG. 11. The magnetoresistance  $\Delta\rho/\rho$  of  $\text{Er}_{0.7}\text{Y}_{0.3}\text{Co}_2$  at 5 (a) and 8 kbar (b) at various values of temperature.

### 3. Magnetization

Figure 13 displays the temperature-dependent magnetization  $M(T)$  of  $\text{Er}_{0.7}\text{Y}_{0.3}\text{Co}_2$  and  $\text{Er}_{0.6}\text{Y}_{0.4}\text{Co}_2$  measured under various values of pressure in low magnetic fields (only zero field-cooled data are presented). Only  $T_C^R$  vs  $P$  can be deduced from these data. In order to resolve  $T_C^{\text{Co}}$  considerably lower fields of about 1 mT are required (compare with Fig. 3). At low fields, however, the signal from the sample cannot be separated with the due accuracy from that of the pressure cell. The pressure variation of  $T_C^R$  was derived from that temperature where  $M(T)$  decreases most rapidly on heating and is shown in the insets of Fig. 13. These values are in good agreement with  $T_C^R$  obtained from the resistivity data taken in zero field.

The pressure-dependent magnetization curves  $M(H)$  at 4.2 K of  $\text{Er}_{0.6}\text{Y}_{0.4}\text{Co}_2$  and  $\text{Er}_{0.7}\text{Y}_{0.3}\text{Co}_2$  are shown in Fig. 14. In order to resolve better the pressure effect on the Co moment only the saturation region above 1 T is displayed. In  $\text{Er}_{0.6}\text{Y}_{0.4}\text{Co}_2$ , the ambient pressure magnetization curve is characterized by a more rapid increase above 5 T. This behavior can be accounted for by the inverse IEM process and is in agreement with the magnetoresistance data [Fig. 5(a)] where the critical field for IEM was determined as 6.5 T. Thus from Fig. 14 it follows that the Co sublattice becomes

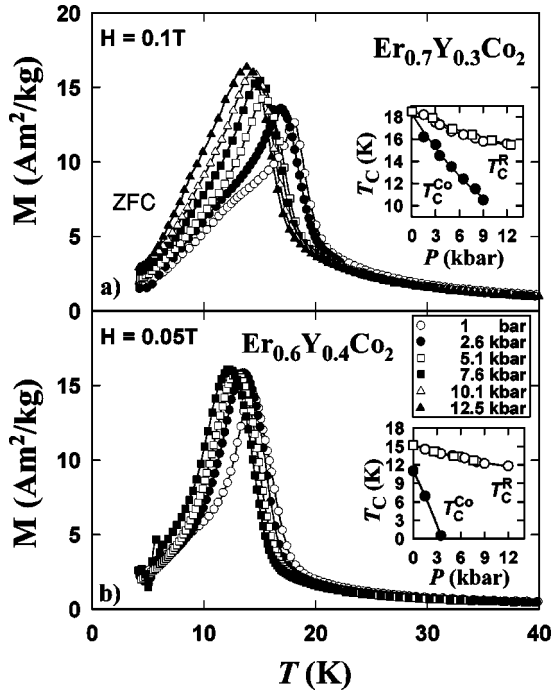


FIG. 13. The temperature-dependent magnetization  $M(T)$  of  $\text{Er}_{0.7}\text{Y}_{0.3}\text{Co}_2$  (a) and  $\text{Er}_{0.6}\text{Y}_{0.4}\text{Co}_2$  (b) at  $H=0.1$  and  $0.05$  T, respectively, under various values of pressure. The inset shows the pressure dependence of the magnetic ordering temperatures  $T_C^R$  and  $T_C^{\text{Co}}$  (open and solid symbols) as deduced from resistivity (circles) and magnetization measurements (squares).

disordered in this compound above 2.6 kbar. The change in  $M$  vs  $P$  is primarily attributed to the pressure dependence of  $\mu_{\text{Co}}$ , yielding  $\partial\mu_{\text{Co}}/\partial P \approx -\frac{1}{2}\partial M/\partial P = -0.013 \mu_{\text{B}}/\text{kbar}$ . Note that the metamagnetic transitions observed are substantially extended over a field range of several teslas. The smearing occurs owing to the large anisotropy of these compounds due to the Er sublattice.

In contrast to the former sample, the magnetization curves of  $\text{Er}_{0.7}\text{Y}_{0.3}\text{Co}_2$  do not interfere up to 9 T for various values of pressure. For  $P=8$  kbar, magnetoresistance data exhibit inverse IEM near to 6 T at 4.2 K [see Fig. 11(b)]. The inset in Fig. 14 displays a nonmonotonic slope of  $M(H)$  in the field range between 5 and 9 T for  $\text{Er}_{0.7}\text{Y}_{0.3}\text{Co}_2$  with a maximum at 7.6 kbar. The maximal value of  $\partial\mu_{\text{Co}}/\partial P$  is equal to that of  $\text{Er}_{0.6}\text{Y}_{0.4}\text{Co}_2$  at ambient pressure (in which inverse IEM occurs at 6.5 T). It was therefore concluded that at  $P$

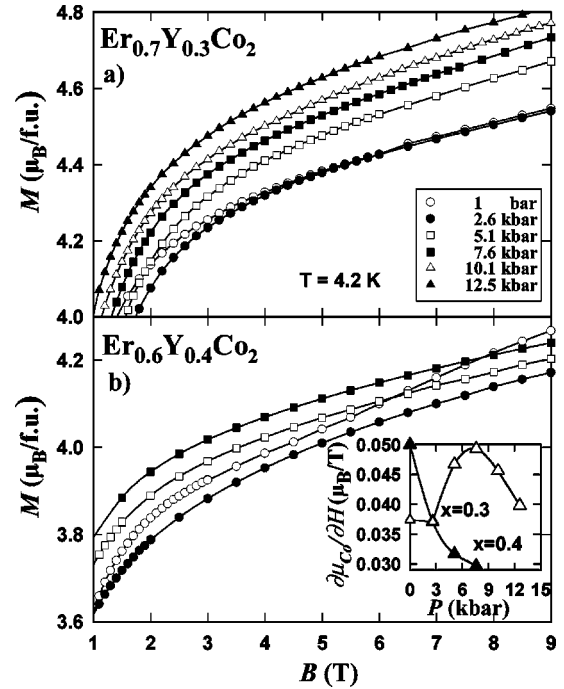


FIG. 14. The field-dependent magnetization  $M(H)$  of  $\text{Er}_{0.7}\text{Y}_{0.3}\text{Co}_2$  (a) and  $\text{Er}_{0.6}\text{Y}_{0.4}\text{Co}_2$  (b) at  $T=4.2$  K under various values of pressure in an extended view. The inset shows the pressure dependence of  $\partial\mu_{\text{Co}}/\partial H$  as obtained from the high-field slope.

$=7.6$  kbar inverse IEM of the Co sublattice occurs also in  $\text{Er}_{0.7}\text{Y}_{0.3}\text{Co}_2$  in the field range between 5 and 9 T (in accordance with the magnetoresistance data). Nevertheless, due to the reduction of the Co sublattice magnetization under pressure along with the smearing effect, no crossover is observed in this field range at the transition.

Table II summarizes the initial pressure dependences of the characteristic temperatures of  $\text{Er}_{1-x}\text{Y}_x\text{Co}_2$  deduced from a linear fit to the data at low pressures. The values for the different Grüneisen parameters  $\Omega_{T_C} = -\partial \ln T_C / \partial \ln V$  (which equals  $\Omega_{T_C^R}$  when both types of magnetic order are well separated in temperature),  $\Omega_{T_C^{\text{Co}}}$ , and  $\Omega_{T_0}$  were deduced by using the values of  $\kappa_S=0.92$  and  $1.2 \text{ Mbar}^{-1}$  for  $\text{ErCo}_2$  and  $\text{YCo}_2$ , respectively,<sup>22</sup> and by interpolation among them.

The values deduced for  $\Omega_{T_C}$  are one order magnitude larger than those, e.g., known for the isostructural  $\text{RAl}_2$  compounds ( $\Omega_{T_C} \approx 4$ ), where only the R sublattice orders

TABLE II. The initial slopes of the pressure dependence of  $T_C$  ( $T_C^R$ ),  $T_C^{\text{Co}}$ , and  $T_0$  are estimated from a linear fit to the first data points.  $\Omega_{T_C}$ ,  $\Omega_{T_C^{\text{Co}}}$ , and  $\Omega_{T_0}$  are deduced by interpolating between the values of  $\kappa_S$  for  $\text{ErCo}_2$  and  $\text{YCo}_2$  given by Ref. 22. For the determination of  $P_{\text{cr}}$  and  $P_{\text{cr}'}$  see the text.

$x$	$\partial T_C / \partial P$ (K/kbar)	$\Omega_{T_C}$	$\partial T_C^{\text{Co}} / \partial P$ (K/kbar)	$\Omega_{T_C^{\text{Co}}}$	$\partial T_0 / \partial P$ (K/kbar)	$\Omega_{T_0}$	$P_{\text{cr}}$ (kbar)	$P_{\text{cr}'}$ (kbar)
$x=0.0$	-0.8	-27					17	23
$x=0.1$	-1.0	-29					10	
$x=0.2$	-0.85	-31					6	
$x=0.3$	-0.45	-26	-1.1	-63	-1.3	-62	<1	8
$x=0.4$	-0.35	-25	-2.5	-240	-2.0	-151		<3
$x=0.5$	-0.27	-22						

magnetically.<sup>23</sup>  $\Omega_{T_C}$  increases up to  $x=0.3$  where  $T_C^R \approx T_C^{\text{Co}}$  and decreases for concentrations where Co ordering is unstable. Obviously, the exceptionally high values for  $\Omega_{T_C^{\text{Co}}}$  reflect the instability of the itinerant moment against pressure.

#### IV. DISCUSSION

##### A. Effect of substitution

As the electrical resistivity is sensitive to the magnetic scattering, this property allows us to study the effect of disorder among the magnetic sublattices, especially the breakdown of long-range magnetic order within the Co sublattice (itinerant  $d$ -electron subsystem). The impact of disorder on the resistivity is well reflected in the change of  $\rho(T)$ . When long-range magnetic order occurs in the Er sublattice and  $H_{\text{eff}}^{\text{Co}}$  exceeds  $H_{\text{cr}}$ , the spin fluctuations in the  $d$  subsystem are suppressed. For concentrations below  $x'_{\text{cr}}$  this results in a sharp drop in the resistivity at  $T_C$ . Very characteristic is the strong increase of  $\rho(T)$  when approaching  $T_C$  from the paramagnetic region, which is enhanced when  $x \approx x_{\text{cr}}$ , the critical concentration for the splitting of the single magnetic phase transition into two (cf. Fig. 1). Here the presence of both short-range order within the Er sublattice and enhanced critical spin fluctuations within the itinerant  $d$  subsystem gives rise to strong scattering of the conduction electrons.

Owing to the substitution of Er by Y,  $H_{fd}^{\text{Co}}$  decreases in  $\text{Er}_{1-x}\text{Y}_x\text{Co}_2$ , resulting in different magnetic-concentration-dependent ground states. The concentration variation of the transport, magnetic, and thermodynamic quantities allows us to identify three different regimes.

(i) Up to  $x=0.3$  there exists only one single magnetic phase transition in this system, which is of a first-order type. In this region, the itinerant sublattice orders magnetically concomitant with the Er sublattice ( $T_C = T_C^R = T_C^{\text{Co}}$ ). The value of the induced Co moment, which is related to the spontaneous volume magnetostriction, decreases progressively with decreasing  $H_{fd}^{\text{Co}}$ .

(ii) In the intermediate-concentration region, two separate magnetic phase transitions are present. In the case of  $\text{Er}_{0.6}\text{Y}_{0.4}\text{Co}_2$  a first-order-type transition occurs at  $T_C^{\text{Co}} = 11$  K and a second-order one at  $T_C^R = 14.5$  K. The data collected in Table I show that the induced moment on the Co sites drops down from roughly  $1\mu_B$  in  $\text{ErCo}_2$  to  $\approx 0.6\mu_B$  in  $\text{Er}_{0.6}\text{Y}_{0.4}\text{Co}_2$ .

(iii) On further dilution by Y ( $x \geq 0.5$ ), the Er sublattice only undergoes a magnetic phase transition ( $T_C = T_C^R$ ). However, the itinerant  $d$  subsystem is still affected by the molecular field provided by the intersublattice Er-Co exchange interaction.

The magnetic  $x$ - $T_C$  phase diagram in Fig. 15 summarizes the concentration dependence of the magnetic ordering temperatures of the  $\text{Er}_{1-x}\text{Y}_x\text{Co}_2$  system. A theoretical treatment of this diagram can be done within the molecular field approximation.<sup>10</sup> Neglecting the crystal field effect on the R sites, the magnetization of the R sublattice reads as

$$H_R = (1-x)Ng_J\mu_B J_R B_J \left( \frac{g_J\mu_B J_R}{kT} H_{\text{eff}}^R \right), \quad (4)$$

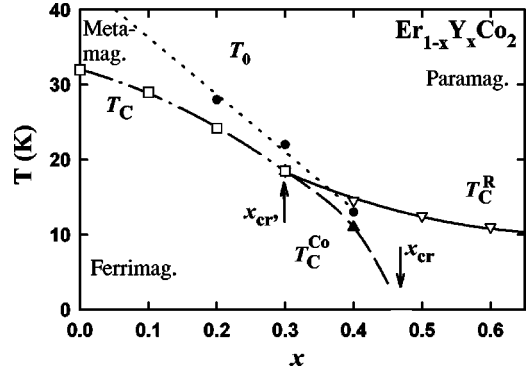


FIG. 15. The magnetic phase diagram of the  $\text{Er}_{1-x}\text{Y}_x\text{Co}_2$  compounds as a function of concentration  $x$ . Dashed-dotted, dashed, and solid lines represent first- and second-order phase boundaries.  $T_0$  limits the temperature range up to which IEM is possible (dotted line; see the text).

where

$$H_{\text{eff}}^R = H_{\text{ext}} + \lambda_{RR}M_R + \lambda_{R\text{Co}}M_{\text{Co}}, \quad (5)$$

and  $\lambda_{RR}$  and  $\lambda_{R\text{Co}}$  are the respective molecular field coefficients. All the other symbols in Eq. (4) have their usual meanings. Here we take  $M_{\text{Co}} > 0$  when  $M_{\text{Co}}$  is oriented opposite to  $M_R$  and  $H_{\text{ext}}$  and, since the intersublattice R-Co interaction is negative,  $\lambda_{R\text{Co}} > 0$ .

For the present analysis the Co sublattice magnetization can be approximated as

$$M_{\text{Co}} = \chi_d H_{\text{eff}}^{\text{Co}} \quad \text{for } H_{\text{eff}}^{\text{Co}} < H_{\text{cr}},$$

$$M_{\text{Co}} = M_{\text{Co}}^{(0)} + \chi_d (H_{\text{eff}}^{\text{Co}} - H_{\text{cr}}) \quad \text{for } H_{\text{eff}}^{\text{Co}} > H_{\text{cr}}, \quad (6)$$

where

$$H_{\text{eff}}^{\text{Co}} = \lambda_{R\text{Co}}M_R - H_{\text{ext}}, \quad (7)$$

$M_{\text{Co}}^{(0)}$  is the Co sublattice magnetization at 0 K, and  $\chi_d$  is the susceptibility of the itinerant  $d$  subsystem. When  $H_{\text{eff}}^{\text{Co}} \leq H_{\text{cr}}$  at  $T = T_C$ , the magnetic transition is of second-order type, and one can write

$$M_R = (1-x) \frac{C}{T} H_{\text{eff}}^R. \quad (8)$$

for  $T > T_C$  with

$$C = \frac{Ng_J^2\mu_B^2 J_R (J_R + 1)}{3k}. \quad (9)$$

Hence, for  $T_C^R$  one obtains

$$T_C^R = (1-x) \frac{Ng_J^2\mu_B^2 J_R (J_R + 1)}{3k} (\lambda_{RR} + \lambda_{R\text{Co}}^2 \chi_d). \quad (10)$$

Considering that  $H_{\text{eff}}^{\text{Co}} = H_{\text{cr}}$  at  $T = T_C^{\text{Co}}$ ,  $T_C^{\text{Co}}$  is related to  $x$  by

$$\frac{H_{\text{cr}}}{(1-x)\lambda_{R\text{Co}}} = Ng_J\mu_B J_R B_J \left[ \frac{g_J\mu_B J_R}{kT_C^{\text{Co}}} \left( \frac{\lambda_{RR}H_{\text{cr}}}{\lambda_{R\text{Co}}} + \lambda_{R\text{Co}}M_{\text{Co}}^{(0)} \right) \right]. \quad (11)$$

Equations (10) and (11) were applied to  $\text{Er}_{0.6}\text{Y}_{0.4}\text{Co}_2$  with  $T_C^{\text{Co}}=11$  K and  $T_C^{\text{Er}}=14.5$  K. Using the parameters for  $\text{YCo}_2$  [ $\chi_d=1.78\times 10^{-3}$  emu/mol,<sup>24</sup>  $M_{\text{Co}}^{(0)}=1$   $\mu_{\text{B}}/\text{f.u.}$ ,  $H_{\text{cr}}=75$  T (Ref. 2)] and taking for  $\text{Er}^{3+}$  ion  $J_{\text{Er}}=15/2$  and  $g_J=6/5$  the following values of the molecular field coefficients were obtained:

$$\lambda_{\text{ErEr}}=0.92 \text{ emu/mol} \quad \text{and} \quad \lambda_{\text{ErCo}}=26.25 \text{ emu/mol.}$$

The critical concentration  $x_{\text{cr}}=0.43$  for  $T_C^{\text{Co}}=0$  was then found from the condition

$$x_{\text{cr}}=1-\frac{H_{\text{cr}}}{Ng_J\mu_{\text{B}}J_{\text{Er}}\lambda_{\text{ErCo}}}, \quad (12)$$

which follows from Eq. 7. Above this concentration, the Co sublattice remains paramagnetic in  $\text{Er}_{1-x}\text{Y}_x\text{Co}_2$  at any temperature. The second critical concentration  $x'_{\text{cr}}$  at which the ordering temperatures of the Er and Co sublattices start to split can be found from the condition

$$\frac{H_{\text{cr}}}{\lambda_{\text{RCo}}}=(1-x'_{\text{cr}})Ng_J\mu_{\text{B}}J_{\text{R}}B_J\left[\frac{g_J\mu_{\text{B}}J_{\text{R}}}{kT_C^{\text{R}}}\left(\frac{\lambda_{\text{R}}H_{\text{cr}}}{\lambda_{\text{RCo}}}+\lambda_{\text{RCo}}M_{\text{Co}}^{(0)}\right)\right]. \quad (13)$$

Using the above numerical values one finds  $x'_{\text{cr}}=0.37$ .

The value of  $\lambda_{\text{ErCo}}$  derived from the Curie temperatures of  $\text{Er}_{0.6}\text{Y}_{0.4}\text{Co}_2$  gives  $H_{\text{ErCo}}^{\text{Co}}=132$  T for the border compound  $\text{ErCo}_2$  and hence predicts the inverse IEM at  $132-75=57$  T and reversal IEM at  $132+75=207$  T. These critical fields are well in agreement with direct magnetization measurements performed under ultrahigh pulse magnetic fields on  $\text{ErCo}_2$ : 52 T (Ref. 18) and 210 T (Ref. 25). This analysis shows that in  $\text{Er}_{1-x}\text{Y}_x\text{Co}_2$  the separate magnetic ordering of the Er and Co sublattices occurs in a very narrow concentration interval  $0.37\leq x\leq 0.43$ . This interval extends with increasing ratio  $\lambda_{\text{RR}}/\lambda_{\text{RCo}}$ .

The solid and dashed-dotted lines in Fig. 15 represent the second- and first-order phase boundaries, respectively, at those concentrations where only one magnetic phase transition takes place in  $\text{Er}_{1-x}\text{Y}_x\text{Co}_2$ . The dashed line shows the concentration dependence of  $T_C^{\text{Co}}$  in the region where  $0<T_C^{\text{Co}}<T_C^{\text{R}}$ . As can be seen, the concentration region found experimentally for the separate sublattice ordering is in agreement with predictions of the above-described model. Solid circles indicate the estimated values for  $T_0$  (the dotted line is a guide for the eye). Below this temperature a conventional itinerant metamagnetic behavior is observed above  $T_C$  and inverse IEM below  $T_C$ . In the case of  $\text{Er}_{1-x}\text{Y}_x\text{Co}_2$  our data reveal a concentration dependence of  $T_0$  (see also Table II).

In order to compare the theoretical magnetic phase diagram of the  $\text{Er}_{1-x}\text{Y}_x\text{Co}_2$  system obtained with the use of Eqs. (10) and (11) with the experimental one, the temperature variations of  $H_{\text{cr}}$  and  $M_{\text{Co}}$  have to be taken into account. The deviations become essential above 20 K. Note that also  $H_{\text{inv}}$  decreases with temperature consistent with the temperature-dependent increase of  $H_{\text{cr}}$  as proposed by the spin-fluctuation theory of Yamada.<sup>19</sup> The concentration dependence of the lattice parameter (from 7.1549 Å in  $\text{ErCo}_2$  to 7.2213 Å in  $\text{YCo}_2$ ) could also have some impact on the

magnetic ordering temperatures since the change in the interatomic distances is equivalent to pressure (either positive or negative). However, using a standard value of the compressibility for all the compounds of this system,  $\kappa\approx 1$   $\text{Mbar}^{-1}$ ,<sup>22</sup> one can evaluate that the lattice expansion when completely replacing Er by Y is equivalent to a positive pressure as high as 25 kbar. As according to Yamada  $\partial H_{\text{cr}}/\partial P\approx +2$  T/kbar,<sup>19</sup> this mechanism should also modify  $H_{\text{cr}}$  essentially.<sup>26</sup> E.g., a similar estimate shows that the difference in the lattice parameters between  $\text{YCo}_2$  and  $\text{LuCo}_2$  corresponds to a chemical pressure of about 42 kbar (the values of  $H_{\text{cr}}$  are nevertheless very close in these compounds).

Although the molecular field approach describes the main details of the magnetic phase diagram given in Fig. 14, it does not take into account the statistical inhomogeneities of the molecular fields being important in the substituted compounds. These inhomogeneities affect the magnetic behavior of the sublattices in the vicinity of the phase transition. In the intermediate compound  $\text{Er}_{0.6}\text{Y}_{0.4}\text{Co}_2$ , both the low-temperature resistivity and the electronic contribution to the specific heat are substantially enhanced with respect to the region  $0\leq x\leq 0.3$ . Both  $\rho_0$  and  $\gamma$  reach the maximum at  $x=0.4$  and decrease on further Y substitution. This indicates that near the critical concentration the itinerant  $d$  subsystem is not fully ordered below  $T_C$  (long-range order is established only inside clusters). Considering  $\rho_0$  and  $\gamma$  as a measure for correlation effects among electrons in this particular compound, this can be referred to  $H_{fd}^{\text{Co}}\leq H_{\text{cr}}$  at  $T=T_C$ . The consequence of strong correlations is the development of critical spin fluctuations in the  $d$  subsystem when  $T_C^{\text{Co}}$  is shifted towards zero, i.e., when  $H_{fd}^{\text{Co}}\leq H_{\text{cr}}$  at  $T=0$ . At low temperatures, the thermally induced spin fluctuations are small and the renormalized properties observed are presumably due to longitudinal spin fluctuations when the criterion for a stable induced moment is nearly fulfilled. The resulting fluctuating Co moments are strongly correlated and act as heavy scatterers for conduction electrons even at lowest temperatures.

However, the absolute value of the enhanced low-temperature resistivity starts to drop as  $H_{fd}^{\text{Co}}$  is further reduced with increasing Y content and the criterion for IEM is far from being fulfilled even at  $T=0$ . This can be understood considering that the mean fluctuating moment at the Co sites is given by the exchange field, and the strength of the correlation effects depends on the proximity to the critical condition for IEM. The existence of a not fully ordered state in the Co sublattice can also be deduced from neutron diffraction studies. A substantial inelastic scattering was observed in this system at 4.2 K in the compounds with  $x>0.4$ , which was attributed to short-range magnetic order within the Co sublattice.<sup>13</sup>

This conclusion is also in agreement with the NMR measurements performed on the isostuctural system  $\text{Er}_{1-x}\text{Lu}_x\text{Co}_2$ .<sup>17</sup> This study revealed a coexistence of both magnetic and nonmagnetic Co sites around the critical concentration. The rise in  $\gamma$  vs  $x$  near the critical concentration is a further indication that the electronic state of the  $d$  subsystem is a subject to changes. The magnetic origin of the low-temperature enhancement of  $\rho(T)$  as well as the existence of clusters can be inferred from the resistivity measure-

ments: below  $T_C^{\text{Co}}$  the application of an external magnetic field results in an irreversible drop of the resistivity.

Finally we want to comment on the weak increase in the volume observed for  $x=0.5$  at  $T=T_C$  which points to a moment of about  $0.2\mu_B$  present at the Co sites. This value corresponds to that directly measured for  $H_{\text{ext}} \leq H_{\text{cr}}$  in the case of  $\text{YCo}_2$ .<sup>2</sup> As under this condition there do not exist stable itinerant  $d$  moments the above value gives a measure for the mean fluctuating moment at the Co sites.

### B. Effect of pressure

As follows from the values of  $\partial T_C / \partial P$ , the pressure effect on the magnetic behavior of the  $\text{Er}_{1-x}\text{Y}_x\text{Co}_2$  compounds is primarily related to the characteristics of the itinerant  $d$  subsystem. Therefore, Yamada's model developed for those  $R\text{Co}_2$  compounds with a nonmagnetic  $R$  may also be relevant in the case when the magnetic field acting at the Co sites is provided by the rare earth molecular field.

In the case of  $R\text{Co}_2$  compounds showing a first-order phase transition from a paramagnetic to a ferrimagnetic state it can be expected that the magnetic phase transition will change towards a second-order type at a critical pressure given by the relation  $H_{\text{fd}}^{\text{Co}} = H_{\text{cr}}(P_{\text{cr}}, T_C)$ . Then, up to the next critical pressure where  $H_{\text{fd}}^{\text{Co}} = H_{\text{cr}}(P_{\text{cr}}, 0)$  the two magnetic sublattices will order separately. Clear evidence for such a pressure-induced splitting of the magnetic ordering can be taken from the data on  $\text{Er}_{0.7}\text{Y}_{0.3}\text{Co}_2$ , which show one first-order type transition at ambient pressure. The pressure variation of  $T_C^{\text{R}}$  for this compound is reflected by  $\partial \rho / \partial T$  vs  $T$  and by a maximum in the slope of  $M(T, P)$ , whereas the separate behavior of  $T_C^{\text{Co}}$  is given by the step in  $\rho(T)$ . Note that also the low-temperature resistivity starts to rise with pressure, reflecting the gradual increase of disorder in the Co sublattice.

A further destabilization of the Co magnetic state occurs in  $\text{Er}_{0.6}\text{Y}_{0.4}\text{Co}_2$ , where the properties at ambient pressure resemble those of  $\text{Er}_{0.7}\text{Y}_{0.3}\text{Co}_2$  at  $P \approx 8$  kbar. In the former compound  $T_C^{\text{Co}}$  vanishes at  $P > 2$  kbar. The low-temperature resistivity reaches a maximum for  $P = 8$  kbar, thus giving the upper limit for  $P_{\text{cr}}$ . On further raising pressure the low-temperature hump in  $\rho(T)$  diminishes progressively. The pressure induced magnetic disorder in the Co sublattice can also be traced when considering the pressure-dependent variation of  $\partial M_{\text{Co}} / \partial H$  (see Fig. 14). At 4 K, this quantity crosses a maximum in  $\text{Er}_{0.7}\text{Y}_{0.3}\text{Co}_2$  at about 8 kbar, indicating that inverse IEM takes place in the field range 5–9 T. From the variation of the spontaneous magnetization with pressure we deduce that the change in the magnetic moment at IEM corresponds to about  $0.5\mu_B/\text{f.u.}$ , a value which is close to the measured jump of  $0.54\mu_B/\text{f.u.}$  obtained for  $\text{YCo}_2$ .<sup>2</sup> Note also that the difference in the Co moment for  $x=0.4$  and  $0.3$  deduced from thermal expansion measurements yields  $0.52\mu_B/\text{f.u.}$  (cf. Table II).

In  $\text{ErCo}_2$ , the evolution of the  $\rho(T)$  curves under pressure shows the same features as those of the substituted compounds. The low-temperature resistivity increases gradually under pressure with a maximum value at about 23 kbar, above which the hump in resistivity diminishes. As was discussed in the above section,  $\rho_0$  as a function of concentration

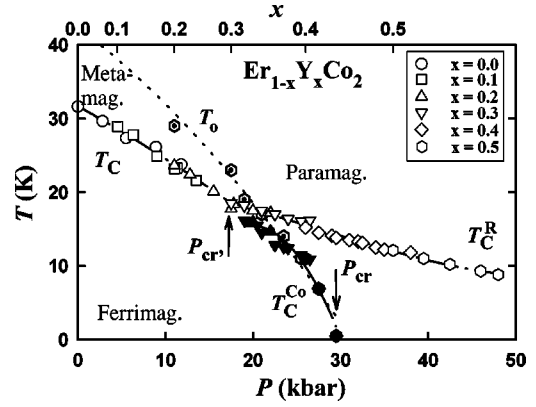


FIG. 16. The magnetic phase diagram observed for  $\text{Er}_{1-x}\text{Y}_x\text{Co}_2$  as a function of pressure  $P$ . Dashed-dotted, dashed, and solid lines represent first- and second-order phase boundaries.  $T_0$  limits the temperature range up to which IEM is possible (dotted line; see the text).

reaches a maximum for the critical concentration  $x_{\text{cr}}$  where  $T_C^{\text{Co}} \rightarrow 0$ . The same conclusion can also be drawn from the pressure-dependent variation of this quantity, i.e., that  $\rho_0$  peaks for  $P_{\text{cr}}$ . From this comparison it is supposed that in  $\text{ErCo}_2$  the Co sublattice also orders separately in a narrow pressure range at about 20 kbar, while for higher pressures the Er sublattice orders only. It is interesting to note that also  $\Omega_{T_C^{\text{Co}}}$  and  $\Omega_{T_0}$  are exceptionally large for  $x=0.4$ , which is close to  $x_{\text{cr}}$  and where  $P_{\text{cr}} \approx 2$  kbar, and that both values are close to each other.

A quantitative comparison with the spin-fluctuation theory given by Yamada can be done when considering the pressure variation of the critical field ( $\partial H_{\text{cr}} / \partial P \approx +2$  T/kbar) which is in a fair agreement with  $\partial H_{\text{inv}} / \partial P = -1.8$  and  $-3$  T/kbar deduced for  $\text{Er}_{0.7}\text{Y}_{0.3}\text{Co}_2$  and  $\text{Er}_{0.6}\text{Y}_{0.4}\text{Co}_2$ , respectively. Furthermore, for  $\text{ErCo}_2$  taking the direct measured  $H_{\text{inv}} = 52$  T and the critical pressure for magnetic order of the Co sublattice  $P_{\text{cr}} \approx 23$  kbar, one can roughly estimate  $\partial H_{\text{inv}} / \partial P = -2.3$  T/kbar which is also in agreement with the theory. Neglecting the pressure variation of the intersublattice molecular field  $H_{\text{ErCo}}^{\text{Co}}$  and assuming that the parameters of the itinerant subsystem are the same as in  $\text{YCo}_2$  throughout the investigated series, the critical condition for the “splitting” of the transition temperatures can be written in the form

$$H_{\text{fd}}^{\text{Co}}(T_C, x) = H_{\text{cr}}(T_C, P). \quad (14)$$

This equation shows that the decrease of  $H_{\text{fd}}^{\text{Co}}$  by Y substitution acts in the same way as the increase  $H_{\text{cr}}$  by application of pressure: in both the cases  $H_{\text{fd}}^{\text{Co}}$  can be made smaller than  $H_{\text{cr}}$ . Considering Eqs. (10) and (11) one can see that the same conclusions hold also for the common Curie points ( $T_C$  or  $T_C^{\text{R}}$ ). Thus, all the transition temperatures of the substituted compounds under pressure correspond to different values of the ratio  $H_{\text{fd}}^{\text{Co}}/H_{\text{cr}}$ .

This observation allows us to combine the pressure dependent data of all the  $\text{Er}_{1-x}\text{Y}_x\text{Co}_2$  compounds as shown in Fig. 16. Here, the various pressure-dependent characteristic temperatures of the substituted compounds are positioned in such a way that they match each other, thus resulting in a

unified phase diagram (for  $\text{ErCo}_2$  we have only taken the data obtained from the liquid-pressure cell measurement). The solid and dashed-dotted lines represent the second- and first-order phase boundaries, respectively, and  $P_{\text{cr}}$  and  $P_{\text{cr}'}$  mark the respective critical pressures. The dotted line follows the estimated values for  $T_0$ . Note that closely related phase diagrams have also been established from pressure-dependent measurements on  $\text{Fe}_2\text{P}$ ,  $\text{HfFe}_2$ , and  $\text{CoS}_2$ , all compounds exhibiting a single first-order magnetic phase transition at  $T_C$ .<sup>27–29</sup> These compounds behave similarly, i.e., a pressure-induced splitting of the first-order type phase transition in the same way as by substitution for  $(\text{Fe}_{1-x}\text{Mn}_x)_2\text{P}$  and  $(\text{Hf}_{1-x}\text{Ta}_x)\text{Fe}_2$ , and a pressure dependent  $T_0$  for  $\text{CoS}_2$ .<sup>29–33</sup>

The phase diagram in Fig. 15 is plotted in a linear scale with respect to pressure. As can be seen, in this case the concentration scale is not linear. Plotting  $x$  vs  $P$  one finds that the  $T_C(P)$  dependence corresponds to  $T_C(x^{4/3})$ . Since the molecular field  $H_{\text{fd}}^{\text{Co}}$  varies linearly in function of  $x$ , this gives, in particular, the pressure variation of  $H_{\text{cr}}$  proportional to  $P^{4/3}$ .

## V. SUMMARY

Long-range magnetic order in the  $\text{Er}_{1-x}\text{Y}_x\text{Co}_2$  compounds is driven by the Er sublattice, and the itinerant  $d$  subsystems orders when the critical condition for IEM is fulfilled. Either a single or two distinct magnetic phase transitions are observed depending on the ratio of  $H_{\text{fd}}^{\text{Co}}/H_{\text{cr}}$ , which can be varied by temperature, pressure, and Er/Y substitution. The presence of two magnetic phase transitions,

where the Er sublattice orders at temperatures higher than that of the itinerant Co sublattice, is limited with respect to both concentration and pressure. The theoretical analysis shows that the above behavior, a “splitting” of the magnetic phase transition, is common for ferrimagnets with one unstable magnetic sublattice.

In the proximity of the critical point, where the long-range magnetic order of the itinerant sublattice vanishes, large values of  $\gamma$  and  $\rho_0$  are observed, which is caused by strong critical spin fluctuations. These presumably longitudinal spin fluctuations arise when the condition for IEM is nearly fulfilled, i.e.,  $H_{\text{fd}}^{\text{Co}} \leq H_{\text{cr}}$ . Above this critical point only the Er sublattice orders and both  $\gamma$  and  $\rho_0$  drop down.

Itinerant electron metamagnetism was found to be limited by a characteristic temperature  $T_0$  which is sensitive to both concentration and pressure. Depending on the values of  $T_C^R$  and  $T_0$  either a conventional metamagnetic behavior is observed for  $T_C^R < T < T_0$  or inverse IEM occurs for  $T_0 < T < T_C^R$ . In the latter case the induced  $d$  moment is destabilized by an external field higher than the critical value  $H_{\text{inv}}$ .

The data obtained are well understood within the framework of the spin-fluctuation theory of Yamada. There is good agreement with the present experimental data and numerical values calculated within this theory.

## ACKNOWLEDGMENTS

This work was supported by the Austria FWF, Project Nos. P11239 and P12899, and GA ASCR, Project No. A1010811.

- 
- <sup>1</sup>R. Lemaire, *Cobalt* (Engl. Ed.) **32**, 201 (1966).  
<sup>2</sup>T. Goto, K. Fukamichi, T. Sakakibara, and H. Komatsu, *Solid State Commun.* **72**, 945 (1989).  
<sup>3</sup>T. Goto, T. Sakakibara, K. Murata, H. Komatsu, and K. Fukamichi, *J. Magn. Magn. Mater.* **90&91**, 700 (1990).  
<sup>4</sup>E.P. Wohlfarth and P. Rhodes, *Philos. Mag.* **7**, 1817 (1962).  
<sup>5</sup>H. Yamada, J. Inoue, K. Terao, S. Kanda, and M. Shimizu, *J. Phys. F* **14**, 1943 (1984).  
<sup>6</sup>J. Beille, D. Bloch, and J. Voiron, *J. Magn. Magn. Mater.* **7**, 271 (1978).  
<sup>7</sup>W. Steiner, E. Gratz, H. Ortbauer, and H.F. Camen, *J. Phys. F* **8**, 1525 (1978).  
<sup>8</sup>E. Gratz, A. Lindbaum, A.S. Markosyan, H. Müller, Yu. Sokolov, *J. Phys.: Condens. Matter* **6**, 6699 (1994).  
<sup>9</sup>E. Gratz, R. Hauser, A. Lindbaum, M. Maikis, R. Resel, G. Schaudy, R.Z. Levitin, A.S. Markosyan, I.S. Dubenko, A.Yu. Sokolov, and S.W. Sochovsky, *J. Phys.: Condens. Matter* **7**, 597 (1995).  
<sup>10</sup>R.Z. Levitin, A.S. Markosyan, and V.V. Snegirev, *Phys. Met. Metallogr.* **57**, 56 (1984).  
<sup>11</sup>V.V. Aleksandryan, N.V. Baranov, A.I. Kozlov, and A.S. Markosyan, *Phys. Met. Metallogr.* **66**, 50 (1988).  
<sup>12</sup>N.H. Duc, T.D. Hien, P.E. Brommer, and J.J.M. Franse, *J. Phys. F* **18**, 275 (1988).  
<sup>13</sup>N.V. Baranov, A.I. Kozlov, A.N. Pirogov, and E.V. Sinitsyn, *Zh. Eksp. Teor. Fiz.* **96**, 674 (1989) [*Sov. Phys. JETP* **69**, 382 (1989)].  
<sup>14</sup>N.V. Baranov, A.I. Kozlov, and A.N. Pirogov, *Phys. Met. Metallogr.* **70**, 40 (1990).  
<sup>15</sup>N.V. Baranov and A.N. Pirogov, *J. Alloys Compd.* **217**, 31 (1995).  
<sup>16</sup>N. Pillmayr, G. Hilscher, E. Gratz, and V. Sechovsky, *J. Phys. (Paris), Colloq.* **49**, 273 (1988).  
<sup>17</sup>H. Wada, T. Mori, M. Shiga, H. Aruga Katori, M.I. Bartashevich, and T. Goto, *Physica B* **201**, 139 (1994).  
<sup>18</sup>M.I. Bartashevich, H. Aruga Katori, T. Goto, H. Wada, T. Maeda, T. Mori, and M. Shiga, *Physica B* **229**, 315 (1997).  
<sup>19</sup>H. Yamada, *Phys. Rev. B* **47**, 11 211 (1993).  
<sup>20</sup>H. Yamada, *J. Magn. Magn. Mater.* **139**, 162 (1994).  
<sup>21</sup>E. Gratz, R. Resel, A.T. Burkov, E. Bauer, A.S. Markosyan, and A. Galatanu, *J. Phys.: Condens. Matter* **7**, 6687 (1995).  
<sup>22</sup>H. Klimker and M. Rosen, *J. Magn. Magn. Mater.* **7**, 361 (1978).  
<sup>23</sup>S. Jakkola, *Phys. Lett.* **50A**, 35 (1974).  
<sup>24</sup>E. Burzo, E. Gratz, and V. Pop, *J. Magn. Magn. Mater.* **123**, 159 (1993).  
<sup>25</sup>I.S. Dubenko, A.K. Zvezdin, A.S. Lagutin, R.Z. Levitin, A.S. Markosyan, V.V. Platonov, and O.M. Tatsenko, *Pis'ma Zh. Eksp. Teor. Fiz.* **64**, 188 (1996) [*JETP Lett.* **64**, 202 (1996)].  
<sup>26</sup>We, however, cannot take into account this effect unambiguously, since the changes in the  $d$  band parameters in this system seem

- to result in effect of the same order.
- <sup>27</sup>H. Fujiwara, H. Kadomatsu, K. Tohma, H. Fujii, and T. Okamoto, *J. Magn. Magn. Mater.* **21**, 262 (1980).
- <sup>28</sup>K. Hoshi, *J. Phys. Soc. Jpn.* **57**, 3112 (1988).
- <sup>29</sup>T. Goto, Y. Shindo, S. Oagwa, and T. Harada, *Physica B* **237&238**, 482 (1997).
- <sup>30</sup>R. Fruchart, A. Roger, and J.P. Senateur, *J. Appl. Phys.* **4**, 1250 (1969).
- <sup>31</sup>H. Fujii, T. Hokabe, K. Eguchi, H. Fujiwara, and T. Okamoto, *J. Phys. Soc. Jpn.* **51**, 414 (1982).
- <sup>32</sup>Y. Nishihara and Y. Yamaguchi, *J. Phys. Soc. Jpn.* **52**, 3630 (1983).
- <sup>33</sup>Y. Nishihara, *J. Magn. Magn. Mater.* **7**, 75 (1978).